Smart Materials and
Structures

PURPOSE-LED
PUBLISHING™

PAPER • OPEN ACCESS

Low-melting-point alloy/polyurethane auxetic composite foam for outstanding impact protection with favorable shape memory effect

To cite this article: Kang Zhang *et al* 2025 *Smart Mater. Struct.* **34** 045025

OPEN ACCESS
IOP Publishing
Smart Materials and Structures
Smart Mater. Struct. **34** (2025) 045025 (13pp)
https://doi.org/10.1088/1361-665X/adcd19

Low-melting-point alloy/polyurethane auxetic composite foam for outstanding impact protection with favorable shape memory effect

Kang Zhang[1,2], Jingchao Jiang[3], Liuchao Jin[1], Qiang Gao[4], Xiaoya Zhai[5], Sicong Zhou[1], Zhenhong Li[2], Jifan Li[2,*] and Wei-Hsin Liao[1,*]

[1] Department of Mechanical and Automation Engineering, The Chinese University of Hong Kong, Hong Kong Special Administrative Region of China, People's Republic of China
[2] Nano and Advanced Materials Institute Limited, Hong Kong Special Administrative Region of China, People's Republic of China
[3] Department of Engineering, University of Exeter, Exeter EX4 4QF, United Kingdom
[4] School of Mechanical Engineering, Southeast University, Nanjing, People's Republic of China
[5] School of Mathematical Sciences, University of Science and Technology of China, Hefei, People's Republic of China

E-mail: jifanli@nami.org.hk and whliao@cuhk.edu.hk

Received 20 December 2024, revised 20 March 2025
Accepted for publication 15 April 2025
Published 25 April 2025

Abstract

High energy dissipation materials are crucial for impact protection gear. Additionally, if these materials also have shape memory property, they can offer a better body fit and increase comfort feeling. Herein, we present a novel auxetic composite foam with ultrahigh specific energy dissipation (SED) and shape memory property, which was prepared by directly foaming with low-melting-point alloy (LMPA) in polyurethane (PU) followed by thermal compression process. Due to the synergetic action of LMPA and auxetic PU foam (APU), APU/LMPA foam showed better energy dissipation than pristine PU foam. The compression test showed the energy dissipation and SED of the APU/LMPA foam were 13.4 times and 4.8 times higher than non-APU foam, respectively. Furthermore, the SED improvement of APU/LMPA foam was much higher than other reported auxetic foams. The impact test demonstrated that APU/LMPA foam with 30% thinner thickness could reduce transmitted peak force by 62.1% compared to non-APU foam. Additionally, APU/LMPA foam exhibited shape memory effect due to the phase transition of LMPA, allowing it to adapt to different body shapes through thermal process. With its outstanding energy dissipation and shape memory properties, this composite foam is highly promising for personal safety protection, offering excellent user experience.

---

[*] Authors to whom any correspondence should be addressed.

Supplementary material for this article is available online

Keywords: auxetic foam, low melting point alloy, negative Poisson's ratio, specific energy dissipation, shape memory effect

1. Introduction

High performance protective material used in impact protection gear should be able to dissipate larger amounts of energy with equal or smaller mass when compared to other materials [1–4]. This is crucial in protecting individuals from impact and collision forces. To achieve a higher energy dissipation per unit mass (specific energy dissipation, SED), mechanical properties, interfaces between the different phases in a composite material, and structural geometry of the material should be carefully selected [5–9]. Moreover, for personal protective gear, there are usually only a few size options available. Since everyone has a different body shape, it is difficult to achieve a proper fit, leading to discomfort for the user. The auxetic structure design is a promising method to improve the SED and body fit performance of materials due to its negative Poisson's ratio (NPR). Unlike the traditional materials with positive Poisson's ratio, materials with NPR structures form a concave surface when bending out-of-plane. This unique property helps the materials conform to similarly concave surfaces at human body areas, offering excellent body fit if the concave shape can be fixed. For the SED improvement of materials with auxetic structures, Fan *et al* reported an auxetic nylon foam with 2.7 times SED higher than pristine nylon foam [10]. Zeng and Li found that the SED of auxetic PU (APU) foam had SED 1.9 times higher than non-APU foam [11]. However, in some cases, incorporating auxetic structures into foam may result in a decrease in SED, which is because the auxetic foam usually has a higher density, resulting in a higher mass per unit volume. As a result, the SED may decrease even though the overall energy dissipation capabilities of the material have improved. For example, Chen *et al* presented an auxetic LDPE foam with density of 120 kg m^{-3} having only around 75% SED of the non-auxetic LDPE with density of 29.7 kg m^{-3} [12]. Several attempts have been made to improve the SED performance of auxetic foam by adding fillers in the material. Oh *et al* studied the energy dissipation of graphene oxide-wrapped auxetic foam. Compared with pristine PU foam, the auxetic foam incorporated with two-dimensional graphene oxide showed around 27% higher in SED [13]. Kim *et al* tried to coat PLA film with a highly ordered honeycomb concave micropattern on the surface of auxetic foam and their results showed that SED of this multi-dimension auxetic foam was improved by 8.7% compared with the pristine PU foam [14]. Shear thickening gel (STG) which is a type of non-Newtonian materials is also an effective filler to enhance the specific energy absorption of auxetic foam. As reported in our previous work [15], APU foam with STG showed 40% higher SED than the pristine PU foam. To date, achieving high improvement in SED of auxetic foam is still challenging. Therefore, it is crucial to develop new approaches to manufacture high-specific-energy-dissipation auxetic foam.

The low melting point alloy (LMPA) is a promising class of materials for a wide range of applications, including thermal management, wearable electronics, biomedical devices, and soft robotics [16–20]. This is due to their excellent thermal and electrical conductivity, low phase transition temperature, reversible stiffness, biocompatibility, and other desirable properties. However, the use of LMPA for energy dissipation applications has not yet been fully explored. Recent studies have shown that lattice materials made from LMPA using 3D printing and vacuum casting possess high strength and energy absorption capacity, owing to their intrinsic metallic features [21]. In addition, hydrogel composites containing a heterogeneous rigid phase of LMPA within a soft hydrogel matrix have been shown to dissipate more energy than pristine gels, due to the higher fracture force of the macroscale LMPA skeleton in the composite [22]. The LMPA has also been added to various polymer or polymer sponge, such as PDMS, polyester polyol, PU, silicone elastomer, liquid crystal elastomer, epoxy, and PDMS sponge, to create LMPA-polymer composites by blending LMPA with polymer matrix or placing the polymer sponge into LMPA liquid bath [23–30]. However, the incorporation of LMPA into a polymer matrix or polymer sponge typically leads to an increased composite density, attributable to the high density of LMPA (commonly exceeding 6 g cm^{-3}), resulting in most samples exhibiting a density greater than 1 g cm^{-3}. So far, the development of lightweight auxetic foam with LMPA for achieving high energy dissipation has not been reported.

In this study, we introduced a novel APU/LMPA composite foam with high SED property. The manufacturing process of this APU/LMPA composite foam consisted of incorporating LMPA particles into a PU matrix and directly foaming the LMPA/PU composite to obtain PU/LMPA foam, which was then subjected to the triaxial thermal compression technique. The lightweight APU/LMPA foam, with a density of 0.47 g cm^{-3}, exhibited 13.4 times higher energy dissipation and 4.8 times higher SED compared to non-APU foam. The SED improvement achieved by the developed APU/LMPA foam surpassed that of previously reported auxetic foams in the literature. Finite element analysis (FEA) models have been developed to study the mechanism of energy dissipation improvement by examining the deformation process and stress distribution of APU and APU/LMPA under various compression strains. Impact testing using a drop weight apparatus revealed that the APU/LMPA foam, when 30% thinner, reduced transmitted force by 62.1% in comparison to non-APU foam. Increasing the LMPA particle content enhanced the stiffness of the APU/LMPA foam, thereby further reducing transmitted force. Dynamic mechanical analysis (DMA) results showed that the loss modulus of APU/LMPA foam was greater than that of APU and PU foam, reflecting a higher viscous response and greater dissipation of energy. It was also found that the storage modulus difference between APU/LMPA and APU foam became more pronounced at higher frequencies, potentially due to the hardening effect of LMPA. Furthermore, the as-produced APU/LMPA foam possessed a shape memory effect, which is helpful for the ergonomic design of the protective gear, allowing it to adjust and conform more closely to the user's body contours when heated. The thermo-mechanical and thermal conductive properties of the APU/LMPA composite foam have been studied to gain a deeper understanding of the shape memory mechanism. Consequently, this multifunctional auxetic composite foam holds promise for applications in impact absorption.

2. Materials and methods

2.1. Materials

LMPA (Pb 25 wt%, Sn 12.5 wt%, Bi 50 wt%, Cd 12.5 wt%) with melting point of ~70 °C was purchased from Dongguan Dingguan Metal Technology Co., Ltd, China. Tween-20 was purchased from Sigma-Aldrich Chemical Company. PU foaming solutions (part A and part B) were purchased from Haibeisi Materials Co., Ltd.

2.2. Preparation of LMPA particles

The synthesis schematic diagram of LMPA particles is shown in figure 1(a). Firstly, LMPA and tween-20 as surfactant were added into the hot water at 90 °C for a certain time to make sure that LMPA was completely melted. Then the mixture was ultrasonicated at 1000 W for 20 min to form LMPA droplets. The application of the high ultrasonic power of 1000 W was essential to effectively break the molten LMPA into fine droplets, ensuring an efficient droplet fabrication process that was completed within a relatively short duration of 20 min. Finally, the mixture was quickly cooled in ice water followed by filtering and drying to obtain LMPA particles.

2.3. APU foam preparation

The original PU foam was made by mixing part A (polyol) and part B (diisocyanate) at a weight ratio of 100:40 followed by casting into a mold. The obtained PU foam had density of around 0.19 g cm^{-3} and thickness of 20 mm. For the preparation of APU foam, firstly, the PU foam was put in a home-made aluminum mold with a triaxial compression ratio of 2.1. The mold was then put in an oven for heating at 200 °C for 1 h, and finally cooled down to room temperature to obtain APU. The obtained APU foam had density of around 0.41 g cm^{-3} and thickness of 14 mm.

2.4. Preparation of PU/LMPA and APU/LMPA composite foam

Firstly, LMPA particles were mixed with part A (polyol) of the PU foaming solution and stirred the mixture for 10 min so that the LMPA particles could distribute uniformly in part A. Then the mixture was blended with part B (diisocyanate) with part A/part B weight ratio of 100/40 followed by casting into a mold to form PU/LMPA foam. PU/LMPA foams had thickness of 20 mm. Two PU/LMPA foams with thickness of 20 mm were prepared by adding 10 wt% and 20 wt% LMPA particles, namely PU/10%LMPA and PU/20%LMPA, respectively. PU/10%LMPA and PU/20%LMPA have densities of 0.21 g cm^{-3} and 0.24 g cm^{-3}, respectively. Then two types of PU/LMPA foams were made into APU/LMPA auxetic foams (APU/10%LMPA and APU/20%LMPA) by using the triaxial thermocompression method. APU/LMPA foams had thickness of 14 mm. APU/10%LMPA and APU/20%LMPA have densities of 0.43 g cm^{-3} and 0.47 g cm^{-3}, respectively.

2.5. Characterizations

The microstructures of the LMPA, PU foam, PU/LMPA, APU and APF/LMPA composite foams were investigated by SEM (TM3030Plus, Hitachi). The element mapping of LMPA was acquired using a XFlash660 energy-dispersive EDX detector (Bruker, Germany). Before the SEM characterization, the samples were coated with a thin layer of gold using a gold sputtering coater for 1 min. A Fourier transform infrared spectrometer (FT-IR, PerkinElmer) was used to characterize the chemical bonding states of the PU foam, PU/LMPA, APU and APF/LMPA composite foams through an ATR mode from 4000 to 500 cm^{-1}. Foam samples with 2 cm in width and 2 cm in length were used for the FTIR test to ensure complete coverage of the crystal surface of the ATR accessory. Thermogravimetric results were obtained by a thermogravimetric analyzer (TGA 1000, TA instrument, USA). The x-ray diffraction (XRD, Analytical AERIS) was utilized to characterize the phase structure of PU foam, PU/LMPA, APU and APF/LMPA composite foams. The foam samples were analyzed directly by placing them into the XRD equipment without any additional preparation. The transformation temperatures of foams were measured by differential scanning calorimetry (DSC) on a TAQ2000 instrument. For the DSC analysis, the foam samples were cut into small sizes with weight of around 5 mg. Hardness was determined using a hand-held shore A hardness tester (Guangzhou Lantai Instrument Co., China). Measurement of Poisson's ratio was based on video data acquired with a high-speed camera (Qianyan Lang 5F01, Junda Hi-Tech Co., Ltd) during the compression test performed in the MTS Material Testing System (Model: E43.104). The hysteresis stress−strain curves of the foams were measured by a universal testing machine (LE3104, LiShi (Shanghai) Instruments Co., Ltd.). The dynamic impact test was carried out by a drop weight tester (L223, LiShi (Shanghai) Instruments Co., Ltd). During the process, the drop hammer weighing 2.5 kg fell from

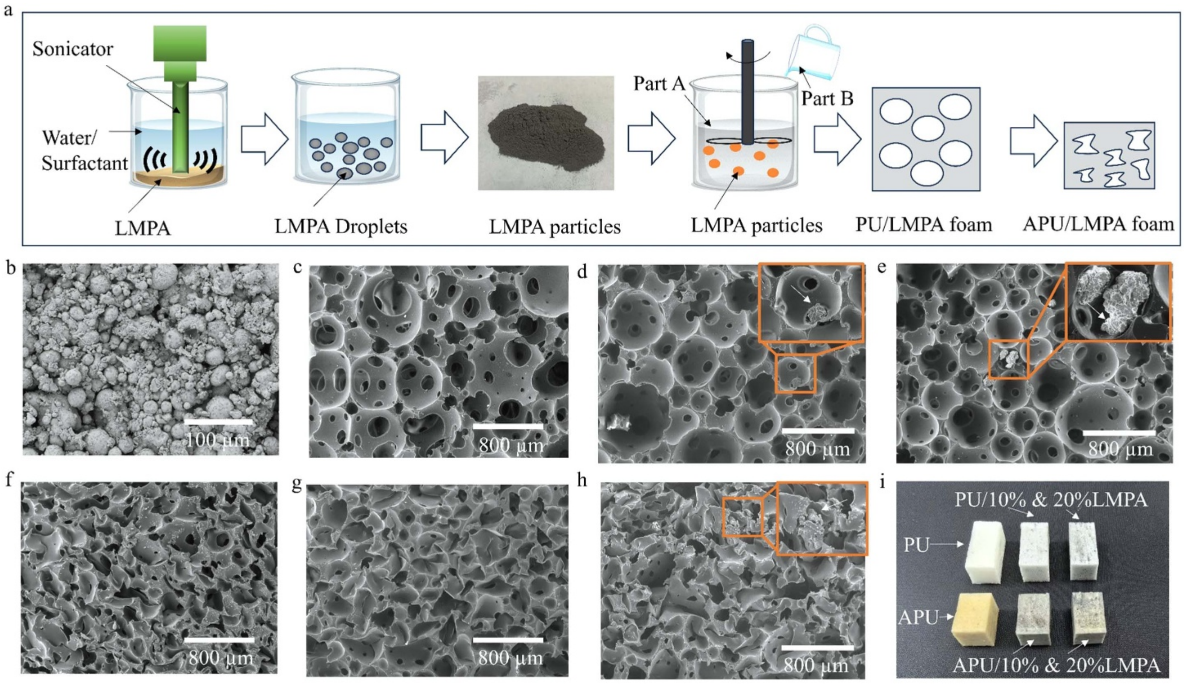

Figure 1. (a) Fabrication schematics of APU/LMPA composite foam. (b)–(h) SEM images of LMPA particles (b), PU (c), PU/10%LMPA (d), PU/20%LMPA (e), APU (f), APU/10%LMPA (g), APU/20%LMPA (h). (i) Photographs of PU, PU/10%LMPA, PU/20%LMPA, APU, APU/10%LMPA and APU/20%LMPA.

height of 204 mm to strike the sample with impact energy of 5 J. DMA (Q800, TA Instrument, USA) was performed at a mechanical dynamic analysis frequency between 0.01 and 100 Hz with 0.5% dynamic strain amplitudes at 25 °C. Abaqus/Explicit solver was employed for calculation of the deformation and stress distribution. The temperature of the sample surface was recorded by a thermal camera (E50, FLIR, USA).

3. Results and discussion

3.1. Microstructures, physicochemical and thermal properties and auxeticity of APU/LMPA composite foam

The fabrication process of LMPA particles using the ultrasonic method and APU/LMPA composite foam using a thermal compression method were schematically shown in figure 1(a). The ultrasonic method was chosen due to its simplicity and high efficiency. The element mapping images of LMPA particles were shown in figure S1, indicating that the LMPA contains Sn, Bi, and Pb elements. The SEM image of LMPA particles was displayed in figure 1(b), and it was observed that most particles were spherical in shape and had particle sizes of less than 100 μm. Figure 1(c) shows the open cell structures that were typical of flexible PU foam. The cell morphology of PU foam with 10 wt% and 20 wt% LMPA were presented in figures 1(d) and (e), respectively. It was observed that PU/10%LMPA and PU/20%LMPA foam had similar pore sizes (figure S2) and cell morphology as pure PU foam, and some LMPA particles were trapped in the cell structures. Interestingly, it was found that the shape of LMPA particles in PU/10%LMPA and PU/20%LMPA foam changed from spherical to irregular, which was attributed to the remelting of LMPA particles at higher temperatures during the PU foaming process. The highest inner temperature during the PU foaming process was observed to be around 95 °C, which was higher than the melting point (∼70 °C) of LMPA, as indicated in figure S3. Attempts were made to add more LMPA particles (30 wt% and 40 wt%) into the PU foam, but it was found that a higher LMPA particle content could interfere with the foaming process, resulting in the collapse of the PU foam and significant distortion of the cell geometry, as shown in figure S4. Therefore, this study focused on the performance of PU foam with 10 wt% LMPA and 20 wt% LMPA. Figures 1(f)–(h) display the SEM images of APU, APU/10%LMPA, and APU/20%LMPA obtained from PU, PU/10%LMPA, and PU/20%LMPA foams using the triaxial thermal compression process, respectively. It was observed that the microstructures of APU, APU/10%LMPA, and APU/20%LMPA exhibited inwardly buckled cell walls and re-entrant auxetic structures. As shown in figure 1(h), LMPA particles were also found to be trapped in the auxetic pore structures. We further compared the hardness of PU, PU/10%LMPA, PU/20%LMPA, APU, APU/10%LMPA and APU/20%LMPA. The results revealed that the hardness of the developed foams was influenced by their microstructures and LMPA content. Figure 2(a) shows that the hardness of APU (15.9 shore A) was significantly higher than that of pristine PU foam (9.8 shore A), which was attributed to the auxetic structures and higher density of APU. Additionally, it was observed

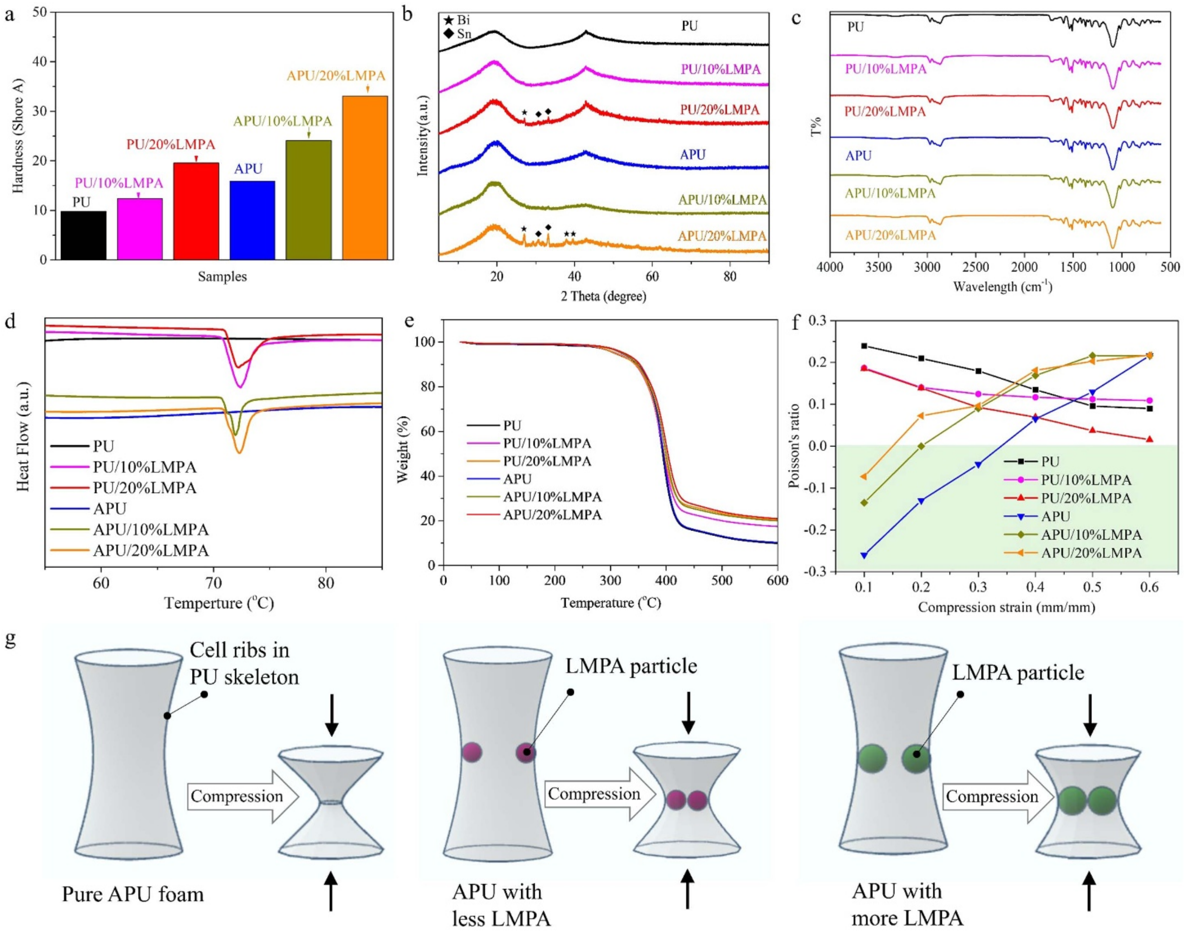

Figure 2. (a)–(e) Shore A hardness (a), x-ray diffraction (XRD) (b), FTIR-spectroscopy (c), differential scanning calorimetry (DSC) curves (d), thermogravimetric analysis (TGA) (e) of PU, PU/10%LMPA, PU/20%LMPA, APU, APU/10%LMPA and APU/20%LMPA. (f) Comparison of Poisson's ratio of PU, PU/10%LMPA, PU/20%LMPA, APU, APU/10%LMPA and APU/20%LMPA under different compression strains. (g) Schematic drawing for the deformation mechanism of APU and APU/LMPA composite foams.

that the hardness of the composite foams increases with an increase in the LMPA content. APU foam with 20 wt% LMPA had hardness (33.1 shore A) around 1.08 times higher than that of APU foam (15.9 shore A). The XRD patterns (figure 2(b)) of the PU/20%LMPA and APU/20%LMPA showed characteristic peaks at 27.2°, 37.9°, 39.7° of Bi and 30.6°, 32.1° of Sn [31], indicating the presence of LMPA. Peaks corresponding to Sn and Bi could not be seen in the XRD plots of PU/10%LMPA and APU/10%LMPA foam due to the low amount of LMPA in the foam and limited instrument sensitivity. The FTIR spectroscopy of PU, APU, PU/LMPA and APU/LMPA composite foams, as presented in figure 2(c), demonstrated that the absorbance peaks of PU/LMPA and APU/LMPA composite foams were similar to those of PU foam. This observation suggested that the presence of LMPA did not lead to thermal oxidation of PU and the high temperature of 200 °C used in the triaxial compression to fabricate the auxetic foam did not result in PU degradation. The DSC curves as shown in figure 2(d) indicated that the LMPA particles existed in PU/LMPA and APU/LMPA composite foams and the LMPA started to melt at about 70 °C, which agreed with the properties of the materials employed in this study. TGA is a widely used technique for investigating the thermal behavior of materials. The TGA analysis of PU/LMPA and APU/LMPA composite foams, as depicted in figure 2(e), revealed that the final weight of the LMPA/PU material was greater than that of pure PU or APU. This observation suggested that LMPA had a higher decomposition temperature than PU. Furthermore, it was observed that the decomposition ratios of PU/LMPA and APU/LMPA composite foams were similar to those of pure PU and APU foam, indicating that the presence of LMPA did not affect the thermal degradation of PU polymer matrix. Figure 2(f) displays the Poisson's ratio as a function of compression strain for PU, APU, PU/LMPA, and APU/LMPA composite foams. The APU and APU/LMPA composite foams exhibited a NPR, which increased with an increase in the compression strain. This result was consistent with previous findings on the strain-dependent Poisson's ratio of auxetic foams [10, 32]. Additionally, the Poisson's ratio of APU/LMPA composite foams was higher than that of pure APU foam. As the LMPA content increased, the Poisson's ratio of APU/LMPA composite foam also increased. For instance, at a compression

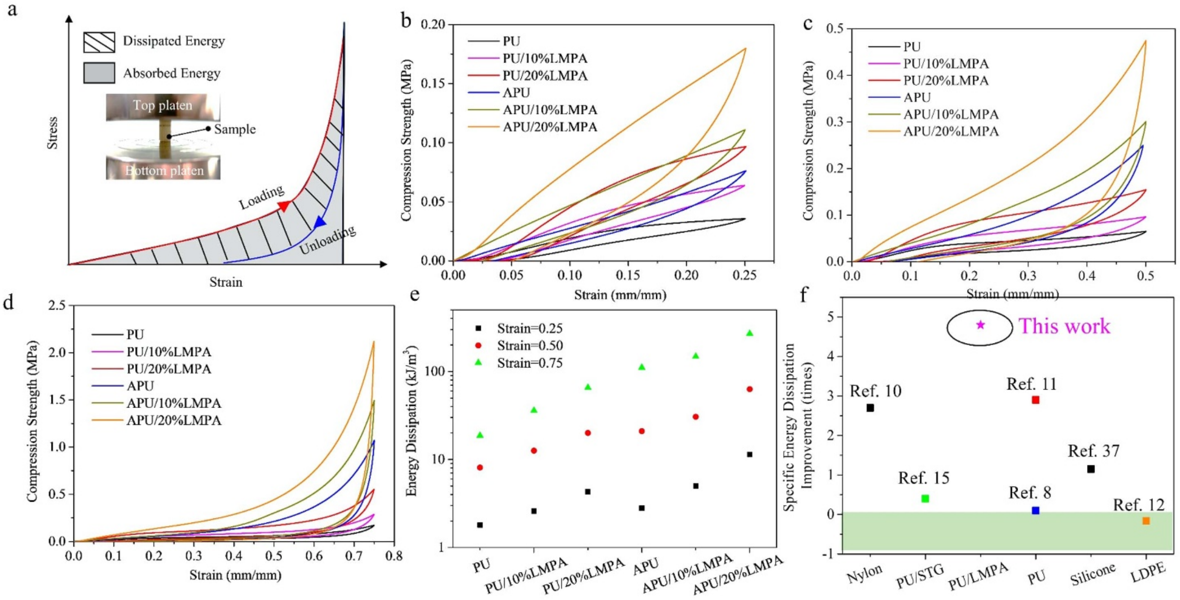

Figure 3. (a) Schematic of quasi-static compression hysteresis test and schematic representation of stress vs strain graph. Absorbed energy is determined by the area under stress–strain curve. Dissipated energy is determined by the area between the loading and unloading stress–strain curve. (b)–(d) Compressive stress–strain hysteresis curves of PU, PU/10%LMPA, PU/20%LMPA, APU, APU/10%LMPA and APU/20%LMPA at compression strain of 0.25 (b), 0.50 (c) and 0.75 (d). (e) Energy dissipation of PU, PU/10%LMPA, PU/20%LMPA, APU, APU/10%LMPA and APU/20%LMPA. (f) Comparison of specific energy dissipation improvement of auxetic materials made by nylon [10], PU/STG [15], PU/LMPA, PU [8, 11], silicone [37], LDPE [12].

strain of 0.1, APU/20%LMPA exhibited a Poisson's ratio of −0.07, while APU/10%LMPA had a Poisson's ratio of −0.14. Figure 2(g) depicts a schematic drawing illustrating the deformation mechanism of APU/LMPA composite foam during compression testing, which explained the aforementioned change in Poisson's ratio. In the case of pure APU foam, the ribs moved inward upon compression, resulting in the NPR effect. However, for APU/10%LMPA, the LMPA particles present in the gap of the reentrant structures prevented the ribs from moving inward over a larger distance, thereby reducing the lateral strain and increasing the Poisson's ratio. Similarly, for APU/20%LMPA, the greater number of LMPA particles in the gap of the reentrant structures further restricted the inward movement of the cell ribs, resulting in a larger Poisson's ratio for the composite foam.

3.2. Quasi-static compression response and energy dissipation of APU/LMPA composite foam

The energy dissipation performance of APU/LMPA composite foam was investigated using quasi-static compression hysteresis testing as shown in figure 3(a). The dissipated energy during compression hysteresis testing can be determined by calculating the area enclosed between the loading and unloading curves, while the SED is defined by dividing the dissipated energy by the mass [33, 34]. In addition to energy dissipation, the energy absorption performance of the composite foam was also discussed. Absorbed energy can be determined by calculating the area under the stress–strain curve during compression (figure 3(a)). Figures 3(b)–(d) present the stress–strain hysteresis curves of PU, APU, PU/10%LMPA, PU/20%LMPA, APU/10%LMPA and APU/20%LMPA composite foams at compression strains of 0.25, 0.50, and 0.75, respectively. As shown in figure 3(d), the PU, PU/10%LMPA, and PU/20%LMPA foams exhibited an initial region of high stiffness, followed by a plateau region. In contrast, APU, APU/10%LMPA, and APU/20%LMPA foams showed an extended region of quasi-linear stiffness up to approximately 35% compression of the foams and did not exhibit a plateau region. The loading curves observed during the quasi-static compression hysteresis testing of the composite foams exhibited a resemblance to those reported for conventional and auxetic foam [35–37]. The Young's modulus of the composite foams, which can be derived from the initial slopes of the stress–strain curves, were also compared with the pristine PU and APU foam as shown in figure S5. The average Young's modulus of APU foam (0.28 MPa) was found to be higher than that of pristine PU foam (0.23 MPa), which was attributed to the presence of auxetic structures in APU foam. The addition of LMPA was observed to increase the Young's modulus of both PU and APU foam, with a higher LMPA content resulting in a greater increase in Young's modulus for the composite foam. The Young's modulus of APU/20%LMPA composite foam was found to be 0.78 MPa, approximately three times that of pristine PU foam. The high stiffness of PU/LMPA and APU/LMPA foam was attributed to the jamming effect of LMPA particles within the foam structures. Figures 3(b)–(d) illustrate that the area of the hysteresis loop increases with an increase in LMPA particle content in PU/LMPA and APU/LMPA composite foam, indicating an improvement in energy dissipation capacity. The energy dissipation values and energy absorption values of PU, APU, PU/LMPA, and APU/LMPA composite foams at compression strains of 0.25, 0.50, and 0.75 were calculated summarized in figures 3(e) and 6. As shown in figure S6, it showed that adding LMPA enhanced the energy absorption performance, with higher LMPA content (20%) leading to greater energy absorption improvements compared to foam with 10% LMPA content. Additionally, APU-based composite foams exhibited superior energy absorption compared to PU-based ones under the same LMPA content and strain conditions. This indicated that both higher LMPA content and the use of APU as a base material contributed to improved energy absorption, particularly at higher strain levels. The energy dissipation values of APU/20%LMPA increased nonlinearly from 11.4 kJ m^{-3} to 63.0 kJ m^{-3} to 269 kJ m^{-3} as the compression strain increases from 0.25 to 0.50–0.75, respectively. This suggested that there was a nonlinear relationship between energy dissipation and compression strain. The energy dissipation value of APU (111 kJ m^{-3}) was found to be 4.9 times higher than that of pristine PU foam (18.7 kJ m^{-3}), while the energy dissipation value of APU/20%LMPA (269 kJ m^{-3}) was found to be 14.4 times that of pristine PU foam (18.7 kJ m^{-3}). These results indicated that the incorporation of LMPA can significantly improve the energy dissipation performance of APU. The SED for APU/20%LMPA (0.57 kJ kg^{-1}), which considered the effect of foam density, was found to be 4.8 times greater than that of pristine PU foam (0.098 kJ kg^{-1}). Furthermore, the SED improvement observed in the APU/LMPA composite foam (4.8 times) was found to be higher than that reported for other auxetic foams in the literature as shown in figure 3(f) and table S1 [8, 10–12, 15, 37]. The highest improvement in SED reported for auxetic foam from polymers such as Nylon, PU, silicone rubber, LDPE, and PU/STG was only found to be 2.7 times.

To illustrate how LMPA particles in the APU/LMPA composite foam contribute to the jamming effect in auxetic foam structures, simplified FEA models were developed using commercial software ABAQUS. FEA models of APU and APU/LMPA structure as compressive examples were shown in figure 4(a). Since it is challenging to replicate the exact re-entrant auxetic model with identical geometries and microstructures as shown in figures 1(f)–(h), the FEA models for APU and APU/LMPA were simplified using representative re-entrant units to study the effect of LMPA particles on the deformation process and stress distribution in auxetic structures.

The two structures were positioned between two rigid plates. The bottom plate was fixed, while the upper plate could move along the compression direction. The friction coefficient between the specimen and the loading platforms was set to 0.2 in the FEA simulation [38–40]. For APU/LMPA model, the LMPA particles (hemispherical shape) were bonded with APU skeletons using a tie constraint. To prevent penetration during loading, the finite element models were configured with a ‘general contact’. The PU material property used in the FEA was determined from the tensile test of three dumbbell samples as shown in figure 4(b). Different hyperelastic material models such as Mooney–Rivlin, Polynomial, Ogden were used to evaluate the PU mechanical experimental data. As shown in figure 4(b), it is clear that Ogden with a strain energy function order of $N = 3$ was the most suitable and stable for the PU material as the Ogden ($N = 3$) fitting curve agrees well with experimental data. For the material property of LMPA, it was assumed to be isotropic, with density of 9670 kg m^{-3}, Young’s modulus of 12 GPa, a Poisson’s ratio of 0.3 and an initial yield stress of 26 MPa. Mesh convergence analysis confirmed that a size of 1 mm provided accurate and stable result as shown in figures 4(c) and S7. The total kinetic energy of the FEA models was much less than the total internal energy throughout the loading process, thus the compression processes of the simulation model could be considered as stable quasi-static analysis. These finite element models examined the deformation process and stress distribution of APU and APU/LMPA under various compression strains (0.2, 0.4 and 0.6). As indicated in figure 4(d), it showed that the presence of LMPA particles appeared to influence the bulking of ribs and stress dispersion under compression. Upon compression with large compression strain, the LMPA particles became jammed together and enhanced the stress distribution by more evenly dispersing stress across the ribs, resulting in an increase in the stiffness and compression stress of the APU/LMPA. The simulation results were supported by experimental outcomes, where prototypes with identical dimensions to the simulation models were tested under varying compression rates. For the APU_model prototype, TPU filament was used. Since 3D printing LMPA directly is challenging, the LMPA portion in the APU/LMPA_model prototype was also printed using TPU filament, despite the different material properties, to maintain identical dimensions. As demonstrated in figure 4(d), it was observed that the experimental results generate a response that is analogous to that of the finite element models. As shown in figure 4(e), the experimental stress–strain curves closely resembled the stress–strain curves from the finite element simulations, demonstrating the simulation’s accuracy in predicting compression behavior. However, the discrepancy between the experimental and simulation results became more significant at higher strain levels. This difference was likely due to defects in the 3D-printed samples, such as the lower strength of TPU compared to LMPA in the actual material and poor adhesion between the printed hemispherical sections and the main structure. Based on the stress–strain curves, it was evident that the addition of LMPA significantly enhances the compressive performance, as indicated by the steeper increase in strength for the APU/LMPA model at higher strain levels. This demonstrates that LMPA improves the material’s load-bearing capacity and resistance to deformation under compression.

3.3. Anti-impact performance and dynamic mechanical properties of APU/LMPA composite foam

To investigate the impact protection performance of APU/LMPA composite foam, a dynamic impact test was conducted using a drop-weight impact system with a striker of

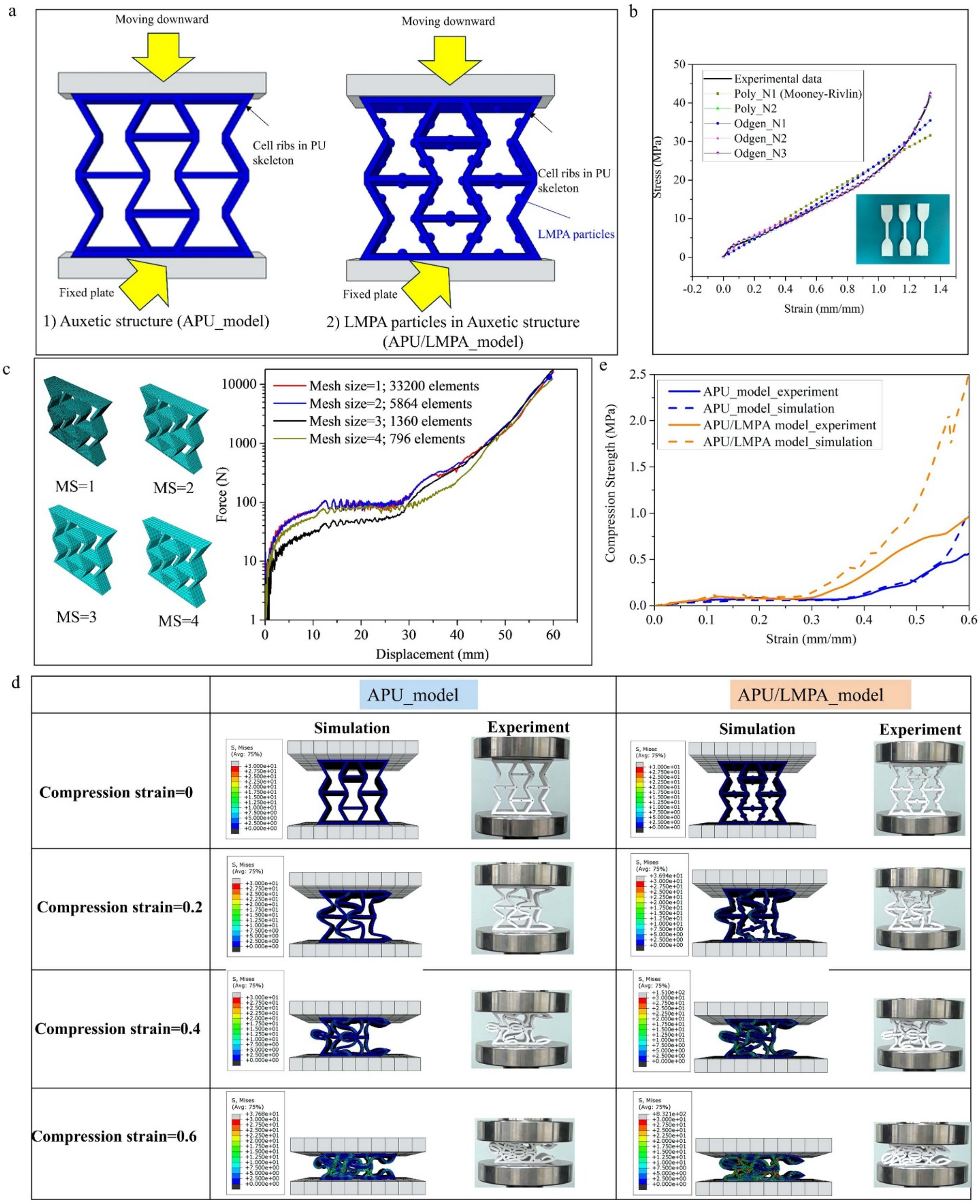

Figure 4. (a) The finite element models of the auxetic structure (APU_model) and LMPA particles in auxetic structure (APU/LMPA_model). (b) The standard tensile specimens of 3D printed PU, experimental and fitted stress–strain curves of hyperelastic models (Mooney–Rivlin, Polynomial, Ogden) for PU. (c) Mesh size convergence testing for the FEA models. (d) Deformation process and stress distribution of APU_model and APU/LMPA_model at compression strains of 0, 0.2, 0.4 and 0.6. (e) The simulation stress–strain curves and experimental stress–strain curves of APU_model and APU/LMPA_model under compression.

2.5 kg and impact energy of 5 J, corresponding to a drop height of 204 mm, in accordance with the ANSI/ISEA 138 standard, which is commonly utilized to evaluate the anti-impact performance of personal protective pads. The samples were positioned on top of an anvil during the impact test, as depicted in figure 5(a), and the transmitted force was measured by a force sensor located underneath. As illustrated in figure 5(b), the peak force of pristine PU foam with a thickness of 20 mm was found to be 2.9 kN. It was also found that the addition of LMPA in PU foam resulted in a reduction

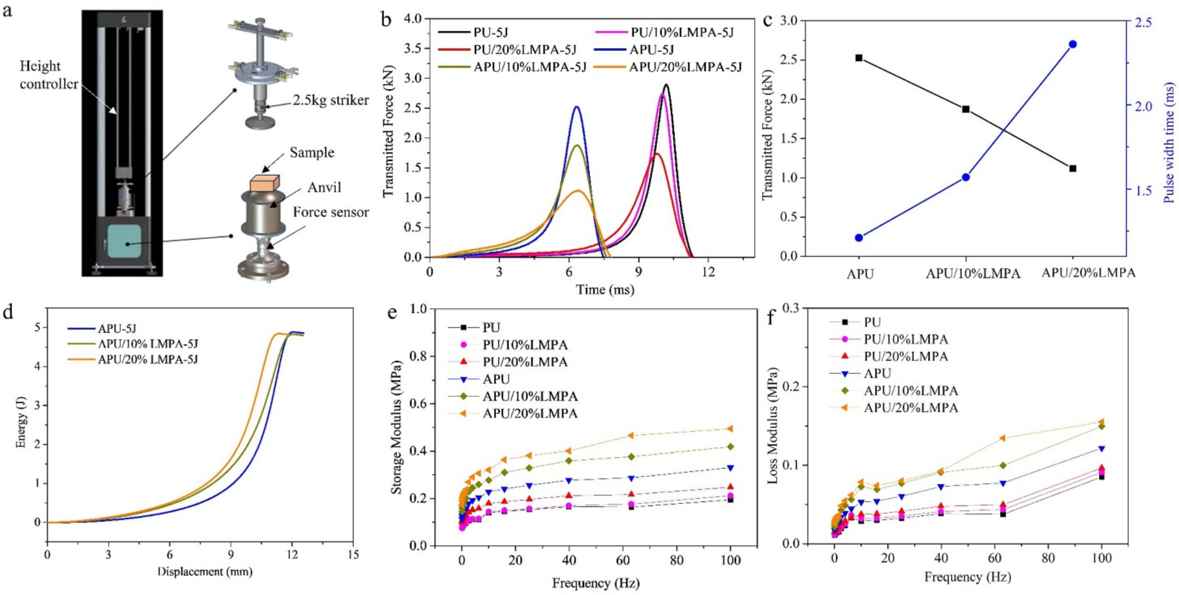

Figure 5. (a) Drop weight impact test machine. (b) Transmitted force–time curves of PU, PU/10%LMPA, PU/20%LMPA, APU, APU/10%LMPA and APU/20%LMPA under impact energy of 5 J. (c) Transmitted peak force and pulse width time of APU, APU/10%LMPA and APU/20%LMPA under impact energy of 5 J. (d) Absorbed energy–displacement curves of APU, APU/10%LMPA and APU/20%LMPA under impact energy of 5 J. (e) Storage modulus and (f) loss modulus for PU, PU/10%LMPA, PU/20%LMPA, APU, APU/10%LMPA and APU/20%LMPA.

of the transmitted peak force. Specifically, the peak force of PU/10%LMPA and PU/20%LMPA decreased to 2.7 kN and 1.7 kN, respectively. APU/20%LMPA with a thinner thickness (14 mm) than pristine PU foam was found to reduce the peak force to 1.1 kN, which was only 27.9% of that of pristine PU foam. These findings suggested that APU/20%LMPA had significant potential for energy dissipation and could be an effective material for protection applications. The results also indicate that an increase in LMPA content corresponds to a decrease in peak force of the APU/LMPA foam, as demonstrated in figure 5(c). The force–time curves of APU/10%LMPA and APU/20%LMPA exhibited a noticeable shoulder peak, as opposed to the narrow peak observed in APU. The broader peaks of the force–time curves suggested that the materials are capable of dissipating impact force over a more extended period, resulting in a lower peak force. As illustrated in figure 5(c), the pulse width time of APU/10%LMPA and APU/20%LMPA were 1.57 ms and 2.36 ms, respectively, which was longer than that of APU (1.21 ms). Figure 5(d) displays the absorbed energy–displacement curves of APU, APU/10%LMPA, and APU/20%LMPA. The results demonstrated that when absorbing the same impact energy, the deformation of APU/20%LMPA foam was lower than that of pure APU, suggesting that the incorporation of LMPA particles in auxetic structures represented an effective structural design. This design allowed for the efficient dissipation and distribution of impact forces, thereby reducing deformation and enhancing the energy absorption capacity of the material. Figures 5(e) and (f) depicte the storage modulus and loss modulus of PU, APU, PU/LMPA and APU/LMPA foams as a function of frequency, within the measuring range of 0.1–100 Hz. The results indicated that an increase in frequency corresponded to an increase in both the storage modulus and loss modulus of the aforementioned foams. It is noted that the storage modulus difference between APU/LMPA and APU foam, as well as the storage modulus difference between PU/LMPA and PU foam, became more pronounced at higher frequencies, potentially due to the hardening effect of LMPA. Additionally, the loss modulus of APU/LMPA foam was greater than that of APU and PU foam, reflecting a higher viscous response and greater dissipation of energy. These findings demonstrated that the incorporation of LMPA in foam structures could enhance the energy dissipation performance of composite foams, as supported by both dynamic and quasi-static tests.

3.4. Shape memory effect of APU/LMPA composite foam

The developed APU/LMPA composite foam was found to exhibit the shape memory effect. Figure 6(a) illustrates the shape memory process of the APU/LMPA composite foam with 20 wt% LMPA. The sequence demonstrated the composite foam's ability to transition between configurations with different curvatures when heated to 120 °C for 5 min (above its melting point of approximately 70 °C) followed by deformation and cooling processes. This process highlighted the APU/LMPA auxetic composite foam's versatility and potential in adaptive protective equipment, accommodating individuals of diverse body shapes. It implied that a single-sized protective pad using the developed composite foam could provide a one-for-all solution. The thermo-mechanical and thermal conductive properties of the APU/LMPA composite

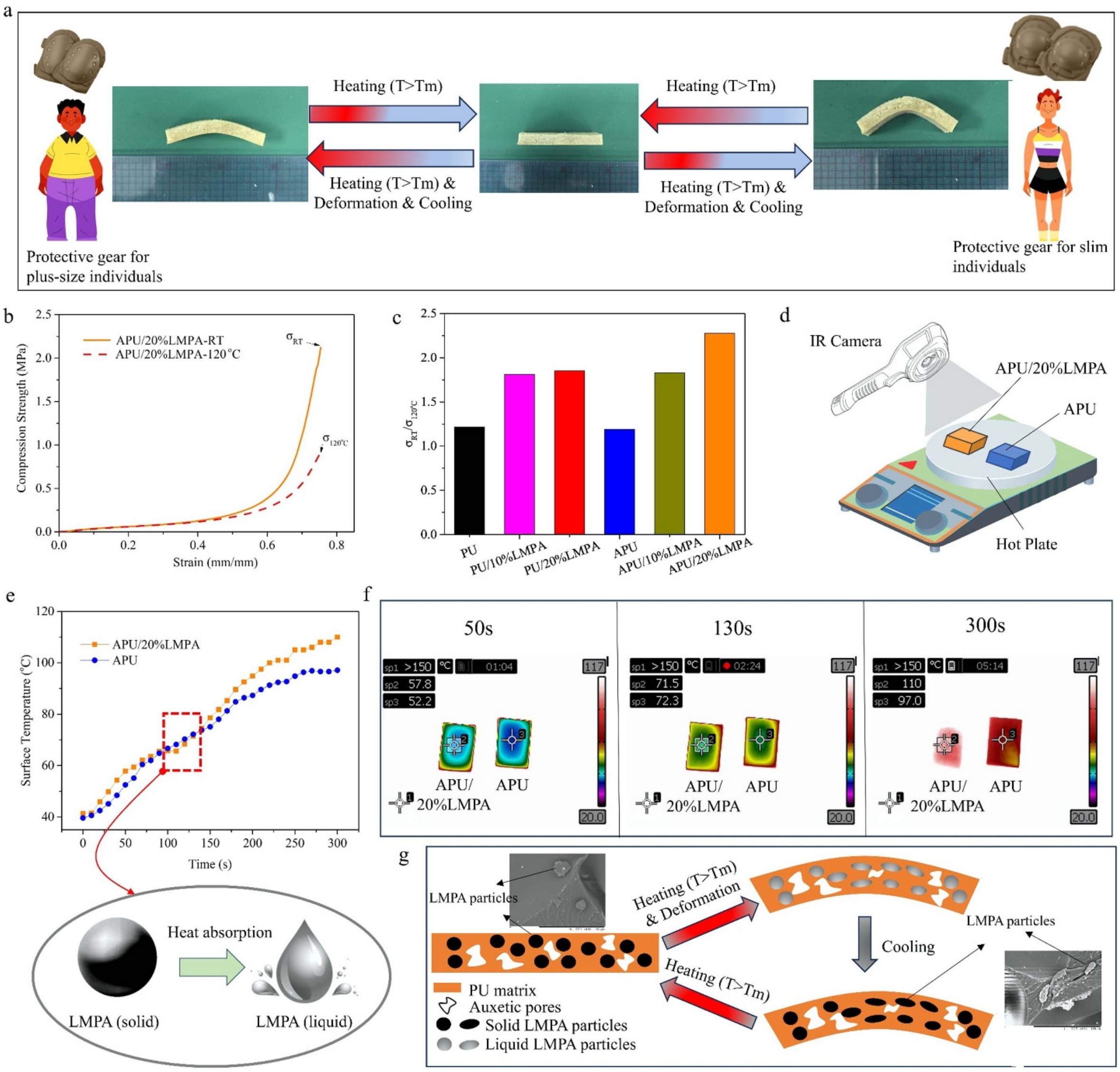

Figure 6. (a) Shape memory effect of APU/20%LMPA. (b) Compressive stress–strain curves of APU/20%LMPA at room temperature and 120 °C. (c) Stiffness variable ratios of PU, PU/10%LMPA, PU/20%LMPA, APU, APU/10%LMPA and APU/20%LMPA. (d) Schematic of the setup for measuring the surface temperature of APU/20%LMPA and APU. (e) Temperature-time curves of APU/20%LMPA and APU. Illustration of the phase change process for LMPA (inside the oval circle). (f) IR thermal images of APU/20%LMPA and APU at 50 s, 130 s and 300 s. Point 1, point 2 and point 3 are on the surface of hot plate, APU/20%LMPA and APU, respectively. (g) Shape memory mechanism of APU/LMPA composite foam and SEM images of APU/20%LMPA foam before and after the shape memory process.

foam have been studied to gain a deeper understanding of the shape memory mechanism. The thermal mechanical characteristics of APU/LMPA were evaluated through quantitative analysis via compression testing at both room temperature and high temperature. The stress–strain curves of APU/20%LMPA at room temperature and 120 °C were presented in figure 6(b). The results indicated that the stress–strain curves overlap during low strain values (<0.3). However, the difference in stress between the two conditions increases as the strain increases. At a compression strain of 0.75, the stress values for APU/20%LMPA at room temperature and 120 °C were found to be 2.1 MPa and 0.92 MPa, respectively. We introduced the stiffness variable ratio as the ratio between stress at room temperature and stress at 120 °C. Figure 6(c) illustrates the stiffness variable ratios of pristine PU and APU foam, as well as PU/LMPA and APU/LMPA composite foams with varying LMPA contents. The results indicated that the stiffness variable ratios of pristine PU and APU foam are 1.20 and 1.19, respectively. However, the stiffness variable ratios of PU/LMPA and APU/LMPA composite foams (10% and 20% LMPA content) were significantly higher, ranging from 1.81 to 2.28. These results indicated that stiffness variation of APU/LMPA composite foams was attributed to the melting of LMPA particles at temperatures above their melting point, instead of the polymer structure changes of PU matrix. We further studied the thermal properties of the APU/LMPA composite foam to evaluate the effect of LMPA particles in the composite foam. The experimental setup involved placing APU/20%LMPA and APU foam samples on a hot plate and recording their surface temperatures using an infrared thermal camera, as presented in figure 6(d). The temperature values and IR thermal images of the two samples were recorded at different heating times, as shown in figures 6(e) and (f). The results indicated that the surface temperature of APU/20%LMPA was approximately 5 °C higher than that of APU after heating for 50 s, which increased to 13 °C when the heating time was 300s. This difference in thermal conductivity was attributed to the higher thermal conductivity of LMPA compared to APU. Interestingly, the surface temperature of APU/20%LMPA was found to be lower than that of APU during a certain heating period, as indicated in the middle figure of figure 6(f) and the area framed in red in figure 6(e), when the heating time was 130 s. For example, at heating time of 130 s, the surface temperature of APU/20%LMPA was 71.5 °C, while that of APU was 72.3 °C. This anomalous temperature zone was found to occur near the melting point of LMPA (∼70 °C). This behavior was attributed to the phase change behavior of LMPA, which allowed it to absorb or release heat without a significant change in temperature. As shown in the insert image in figure 6(e), when LMPA was heated, it underwent a phase change from a solid to a liquid state, absorbing heat in the process, because heat energy was used to break the bonds between the metal atoms, rather than increasing the temperature of the material. Based on the above results, the mechanism of shape memory effect of the developed APU/LMPA composite foam could be explained by figure 6(g). Initially, some LMPA particles were dispersed within the PU matrix of the APU/LMPA composite foam. Upon heating, these LMPA particles were melted into a liquid state. Under applied external force, the voids occupied by the LMPA particles deformed as the liquid LMPA changed shape. During cooling, these reshaped LMPA particles were solidified, fixing the sample into a form with a certain curvature. From the SEM images of the APU/20%LMPA composite foam in figure 6(g), it could be observed that the shape of the LMPA particles changed from spherical to elongated. This morphological transformation provided evidence supporting the proposed shape memory mechanism. When the external force was removed and the sample was reheated, the LMPA returned to a liquid state, allowing the deformed voids to revert to their original shape under the restoring force of the PU matrix. Consequently, the sample returned to its initial shape.

4. Conclusions

In conclusion, this study demonstrated a novel APU/LMPA composite foam that exhibited exceptional SED improvement and favorable shape memory effect. Comprehensive characterization including SEM, XRD, FTIR, DSC, TGA, compression test, drop weight impact test, DMA, high speed camera, IR camera were conducted to analyze the microstructures, mechanical and thermal properties of the APU/LMPA composite foam. The SED improvement (4.8 times) of the APU/LMPA foam was significantly higher than other reported auxetic foams in the literature. The drop weight impact test demonstrated that the APU/LMPA foam could significantly reduce transmitted force compared to non-APU foam, with a 30% thinner foam reducing transmitted force by 62.1%. The superior energy dissipation of APU/LMPA foam compared to pristine PU foam could be attributed to the synergistic effect of LMPA and the NPR of APU, which was also proven by the developed FEA. It was also found that the transmitted peak force of the APU/LMPA foam was reduced as the amount of LMPA increased owing to the higher stiffness arising from LMPA particles in the auxetic structures. The study also revealed that an increase in frequency resulted in a corresponding increase in both the storage modulus and loss modulus of the APU/LMPA foams. Of particular interest, the difference in storage modulus between APU/LMPA and APU foam became more pronounced at higher frequencies. This observation may be attributed to the hardening effect of LMPA. Moreover, the APU/LMPA composite foam displayed the shape memory effect, which implied that a single-sized protective pad made by the APU/LMPA composite foam can provide a one-for-all solution. The shape memory performance of the APU/LMPA composite foam could aid in the ergonomic design of protective gear, enabling it to adjust and conform more closely to the user's body contours when heated. These distinctive attributes rendered the developed multifunctional auxetic composite foam a highly prospective material for utilization in personal protection gear with good user experience.

Data availability statement

The data that support the findings of this study are available upon reasonable request from the authors.

Acknowledgment

This work was supported by The Chinese University of Hong Kong (Project ID: 3110174), the Hong Kong Research Grants Council (Project No. C4074-22G), and the Hong Kong Innovation and Technology Fund (ITP/056/20NP). For the purpose of open access, the authors have applied a Creative Commons Attribution (CC BY) licence to any Author Accepted Manuscript version arising from this submission.

Conflict of interest

The authors declare that they have no known competing financial interests or personal relationships that could have appeared to influence the work reported in this paper.

Author contributions

Kang Zhang: Conceptualization, Formal analysis, Investigation, Methodology, Writing- original draft. **Jingchao Jiang:** Conceptualization, Methodology, Formal analysis. **Liuchao Jin:** Investigation, Methodology. **Qiang Gao:** Investigation, Methodology. **Xiaoya Zhai:** Investigation, Methodology. **Sicong Zhou:** Methodology, Data curation. **Zhenhong Li:** Methodology, Data curation. **Jifan Li:** Conceptualization, Resources. **Wei-Hsin Liao:** Supervision, Resources, Writing—review & editing, Investigation.

ORCID iDs

Kang Zhang https://orcid.org/0000-0001-6110-1217
Jingchao Jiang https://orcid.org/0000-0002-0446-3454
Liuchao Jin https://orcid.org/0000-0001-6204-1922
Wei-Hsin Liao https://orcid.org/0000-0001-7221-5906

References

[1] Yang H, Liu Y, Lu H, Tao R, Wei X and Fu Y 2024 3D-printable Kresling-embedded honeycomb metamaterials with optimized energy absorption capability *Smart Mater. Struct.* **33** 125008

[2] Petelinšek N and Mommer S 2024 Tough hydrogels for load-bearing applications *Adv. Sci.* **11** 2307404

[3] Fan Z Y, Lu L, Sang M, Wu J P, Wang X Y, Xu F, Gong X L, Luo T Z, Leung K C F and Xuan S H 2023 Wearable safeguarding leather composite with excellent sensing, thermal management, and electromagnetic interference shielding *Adv. Sci.* **10** 2302412

[4] Kagias M, Lee S, Friedman A C, Zheng T, Veysset D, Faraon A and Greer J R 2023 Metasurface-enabled holographic lithography for impact-absorbing nanoarchitected sheets *Adv. Mater.* **35** 2209153

[5] Deng Y, Jin Y, Li H and Wang X 2024 A new hybrid auxetic structure capable of uniform deformation exhibits excellent energy absorption *Smart Mater. Struct.* **33** 085031

[6] Wang X Y, Chi H, Che Q L, Zhang F, Wang J R, Zhang H, Wang P X, Liu C, Xu K and Bai Y G 2024 Dynamic H-Bond crosslinking strategy to prepare impact-hardening protective materials with tunable negative Poisson's ratio *Appl. Mater. Today* **36** 102065

[7] Chen Y, Jin Z, Kang W, Liu Z, Yang W and Li Y 2024 3D printed bio-inspired self-similar carbon fiber reinforced composite sandwich structures for energy absorption *Compos. Sci. Technol.* **248** 110453

[8] Yousif H I Y 2012 Auxetic Polyurethane Foam (Fabrication, Properties and Applications) *PhD Dissertation* (available at: https://inis.iaea.org/collection/NCLCollectionStore/_Public/46/131/46131661.pdf)

[9] Zhang Q C, Yu X D, Xia Y Y, Zhang D Y, Lakes R S, Wojciechowski K W and Scarpa F 2024 The shear performance of uniaxially thermoformed auxetic polymer foams *Composites B* **286** 111791

[10] Fan D L, Shi Z Y, Li N X, Qiu J, Xing H P, Jiang Z W, Li M G and Tang T 2020 Novel method for preparing a high-performance auxetic foam directly from polymer resin by a one-Pot CO_2 foaming process *ACS Appl. Mater. Interfaces* **12** 48040–8

[11] Zeng C and Li Y 2019 Material systems and methods of manufacture for auxetic foams *U.S. Patent* 10,479,004 (available at: https://patents.google.com/patent/US10479004B2/)

[12] Chen X Y, Underhill R S and Rodrigue D 2023 A simple method to convert cellular polymers into auxetic metamaterials *Appl. Sci.* **13** 1148

[13] Oh J H, Kim J S and Oh I K 2020 Auxetic graphene oxide-porous foam for acoustic wave and shock energy dissipation *Composites B* **186** 107817

[14] Kim J S, Mahato M, Oh J H and Oh I K 2023 Multi-purpose auxetic foam with honeycomb concave micropattern for sound and shock energy absorbers *Adv. Mater. Interfaces* **10** 2202092

[15] Zhang K, Gao Q, Jiang J C, Chan M S, Zhai X Y, Jin L C, Zhang J F, Li J F and Liao W H 2024 High energy dissipation and self-healing auxetic foam by integrating shear thickening gel *Compos. Sci. Technol.* **249** 110475

[16] Zhao B *et al* 2023 Self-healing liquid metal magnetic hydrogels for smart feedback sensors and high-performance electromagnetic shielding *Nanomicro Lett.* **15** 79

[17] Zhou G, Yao L, Xie Z X, Kamran U, Xie J W, Zhang F, Park S J and Zhang Y H 2023 Controllable construction of CNT-Interconnected liquid metal networks for thermal management *Composites A* **175** 107743

[18] Chen G, Ma B, Zhang J, Chen Y and Liu H 2023 Reprogrammable magnetic soft robots based on low melting alloys *Adv. Intell. Syst.* **5** 2300173

[19] Shen Y F *et al* 2023 Reactive wetting enabled anchoring of non-wettable iron oxide in liquid metal for miniature soft robot *Nat. Commun.* **14** 6276

[20] Mao J, Kim J H and Seo S 2023 Current status and outlook of low-melting-point metals in biomedical applications *Adv. Funct. Mater.* **34** 2307708

[21] Deng F, Nguyen Q K and Zhang P 2022 Liquid metal lattice materials with simultaneously high strength and reusable energy absorption *Appl. Mater. Today* **29** 101671

[22] Takahashi R, Sun T L, Saruwatari Y, Kurokawa T, King D R and Gong J P 2018 Creating stiff, tough, and functional hydrogel composites with low-melting-point alloys *Adv. Mater.* **30** 1706885

[23] Liang S Q, Li Y Y, Chen Y Z, Yang J B, Zhu T P, Zhu D Y, He C X, Liu Y Z, Wang S H and Zhou X C 2017 Liquid metal sponges for mechanically durable, all-soft, electrical conductors *J. Mater. Chem. C* **5** 1586–90

[24] Wang W, Fan Z, Wang J, Wu C, Tang J, Tang L, Zhang D, Xie Z, Cheng Z and Liu Y 2021 Highly conductive liquid metal-based shape memory material with an ultrasensitive fire warning response *ACS Appl. Polym. Mater.* **3** 6027–33

[25] Peng Y, Liu H, Li T and Zhang J 2020 Hybrid metallic foam with superior elasticity, high electrical conductivity, and pressure sensitivity *ACS Appl. Mater. Interfaces* **12** 6489–95

[26] Cai S *et al* 2022 Soft liquid metal infused conductive sponges *Adv. Mater. Technol.* **7** 2101500

[27] Yao B *et al* 2020 Highly stretchable polymer composite with strain-enhanced electromagnetic interference shielding effectiveness *Adv. Mater.* **32** 1907499

[28] Markvicka E J, Bartlett M D, Huang X and Majidi C 2018 An autonomously electrically self-healing liquid metal–elastomer composite for robust soft-matter robotics and electronics *Nat. Mater.* **17** 618–24

[29] Liu H, Tian H, Li X, Chen X, Zhang K, Shi H, Wang C and Shao J 2022 Shape-programmable, deformation-locking, and self-sensing artificial muscle based on liquid crystal elastomer and low–melting point alloy *Sci. Adv.* **8** eabn5722

[30] Xiong S W, Zhang P, Zou Q, Xia Y, Jiang M Y and Gai J G 2021 High thermal conductivity and electrical insulation of liquid alloy/ceramic/epoxy composites through the construction of mutually independent structures *Compos. Sci. Technol.* **202** 108596

[31] Zhang P, Tian R, Zhang X, Ding X, Wang Y, Xiao C, Zheng K, Liu X, Chen L and Tian X 2022 Electromagnetic interference shielding epoxy composites with satisfactory thermal conductivity and electrical insulation performance enabled by low-melting-point alloy layered structure *Composites B* **232** 109611

[32] Zhang Q, Lu W, Scarpa F, Barton D, Rankin K, Zhu Y, Lang Z and Peng H 2021 Topological characteristics and mechanical properties of uniaxially thermoformed auxetic foam *Mater. Des.* **211** 110139

[33] Fu K, Zhao Z and Jin L 2019 Programmable granular metamaterials for reusable energy absorption *Adv. Funct. Mater.* **29** 1901258

[34] Prajapati M J, Kumar A, Lin S C and Jeng J Y 2022 Multi-material additive manufacturing with lightweight closed-cell foam-filled lattice structures for enhanced mechanical and functional properties *Addit. Manuf.* **54** 102766

[35] Allen T, Shepherd J, Hewage T A M, Senior T, Foster L and Alderson A 2015 Low-kinetic energy impact response of auxetic and conventional open-cell polyurethane foams *Phys. Status Solidi b* **252** 1631–9

[36] Vinay V C, Kumar K M and Varma D M 2021 Mathematical modeling of auxetic foams *Mater. Today* **46** 8681–5

[37] Zhang K, Zhang X, Gao Q, Chan M, Zhang S, Li J and Liao W H 2023 Ultrahigh energy-dissipation and multifunctional auxetic polymeric foam inspired by balloon art *Composites A* **167** 107435

[38] Feng G, Li S, Xiao L and Song W 2021 Energy absorption performance of honeycombs with curved cell walls under quasi-static compression *Int. J. Mech. Sci.* **210** 106746

[39] Johnston R and Kazancı Z 2021 Analysis of additively manufactured (3D printed) dual-material auxetic structures under compression *Addit. Manuf.* **38** 101783

[40] Wang W, Zhang W, Guo M, Yang H and Ma L 2024 Impact resistance of assembled plate-lattice auxetic structures *Compos. Struct.* **338** 118132